Electronic Supplementary Information (ESI)

Enhanced electrocatalytic performance of palladium nanoparticles with high energy surfaces in formic acid oxidation

Anna Klinkova,[a] Phil De Luna,[b] Edward H. Sargent,[b] Eugenia Kumacheva,[a] and Pavel V. Cherepanov[c]*

[a] Department of Chemistry, University of Toronto, Toronto, Ontario M5S 3H6, Canada.

[b] Department of Electrical and Computer Engineering, University of Toronto, Ontario M5S 3E4, Canada

[c] Department of Chemical and Biomolecular Engineering, University of Melbourne, Melbourne, VIC 3182, Australia

* Corresponding author, Tel: +61 3 8344 4314, E-mail: pavel.cherepanov@unimelb.edu.au, cherepanov.chem@gmail.com

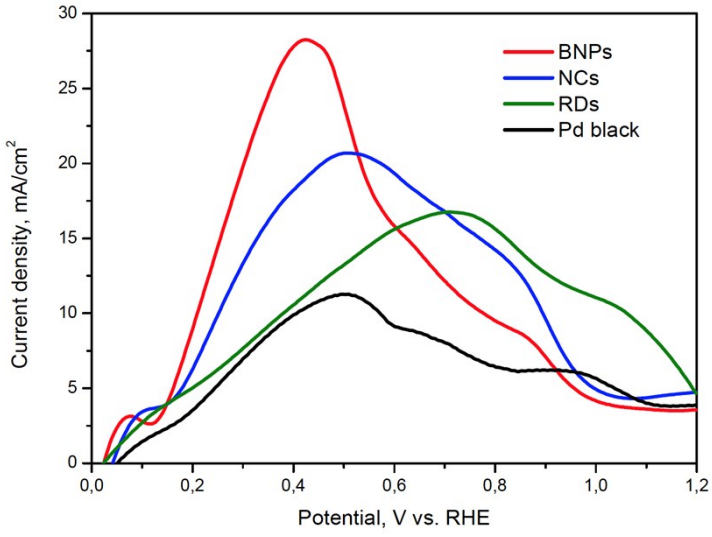

Figure S1. FAO activity of different Pd NPs in Ar-saturated 0.5 M H_2SO_4/ 0.5 M HCOOH solution. Legend: BNPs – branched NPs, NCs – nanocubes, RDs – rhombic dodecahedra NPs, and Pd black. Anodic polarization curves recorded at 50 mV/s scanning rate.

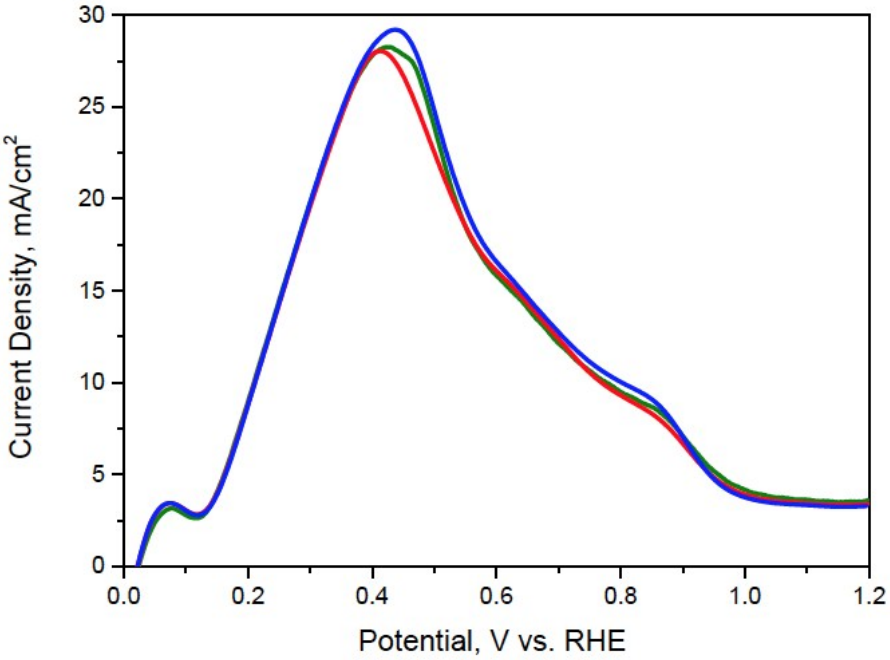

Figure S2. FAO activity of branched NPs in Ar-saturated 0.5 M H_2SO_4/ 0.5 M HCOOH solution. Three anodic polarization curves recorded at 50 mV/s scanning rate.

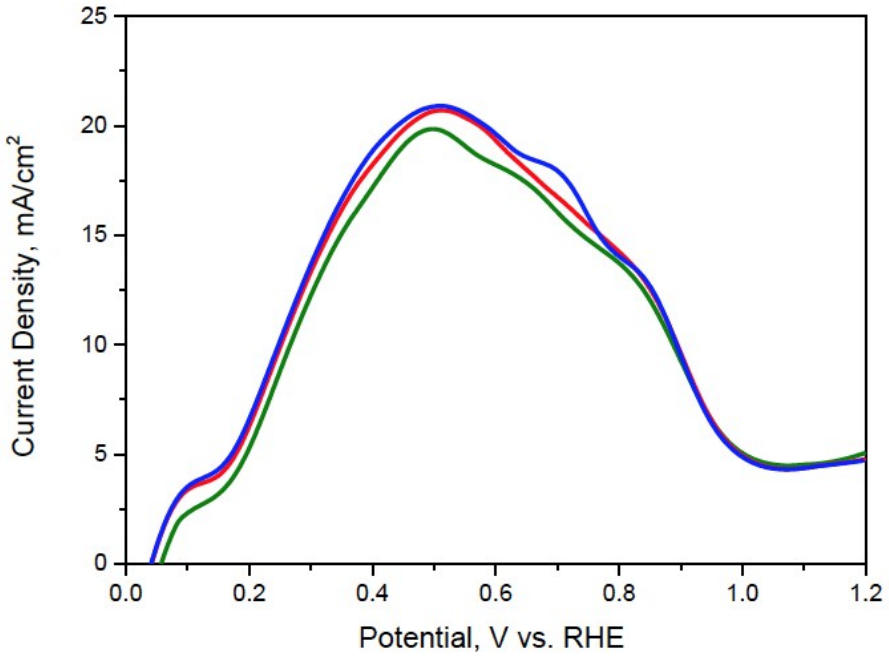

Figure S3. FAO activity of NCs in Ar-saturated 0.5 M H_2SO_4/ 0.5 M HCOOH solution. Three anodic polarization curves recorded at 50 mV/s scanning rate.

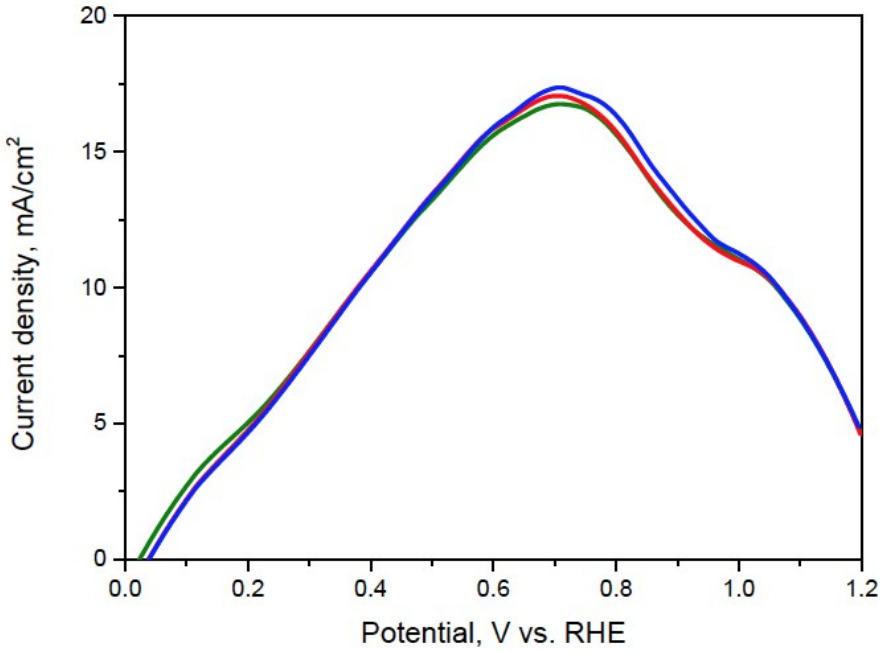

Figure S4. FAO activity of rhombic dodecahedra NPs in Ar-saturated 0.5 M H_2SO_4/ 0.5 M HCOOH solution. Three anodic polarization curves recorded at 50 mV/s scanning rate.

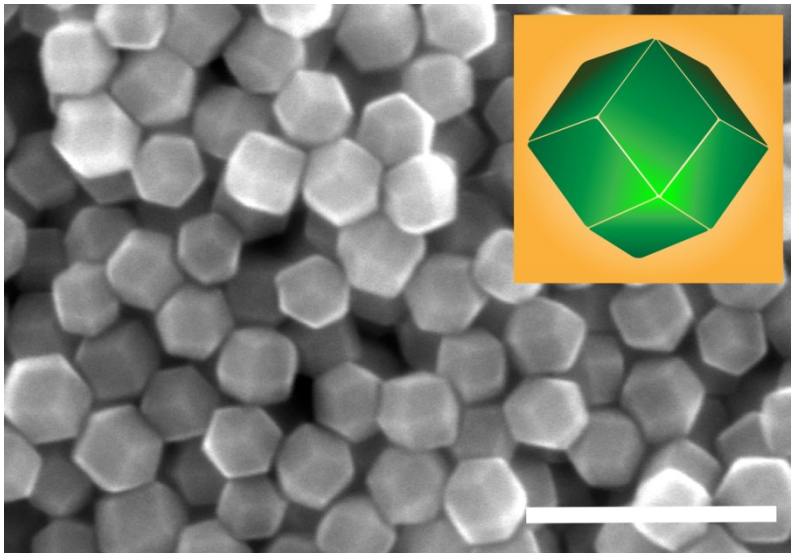

Figure S5. SEM image of rhombic dodecahedra NPs, that were used to measure anodic polarization curves in Figure S1 and S4. Scale bar is 200 nm.

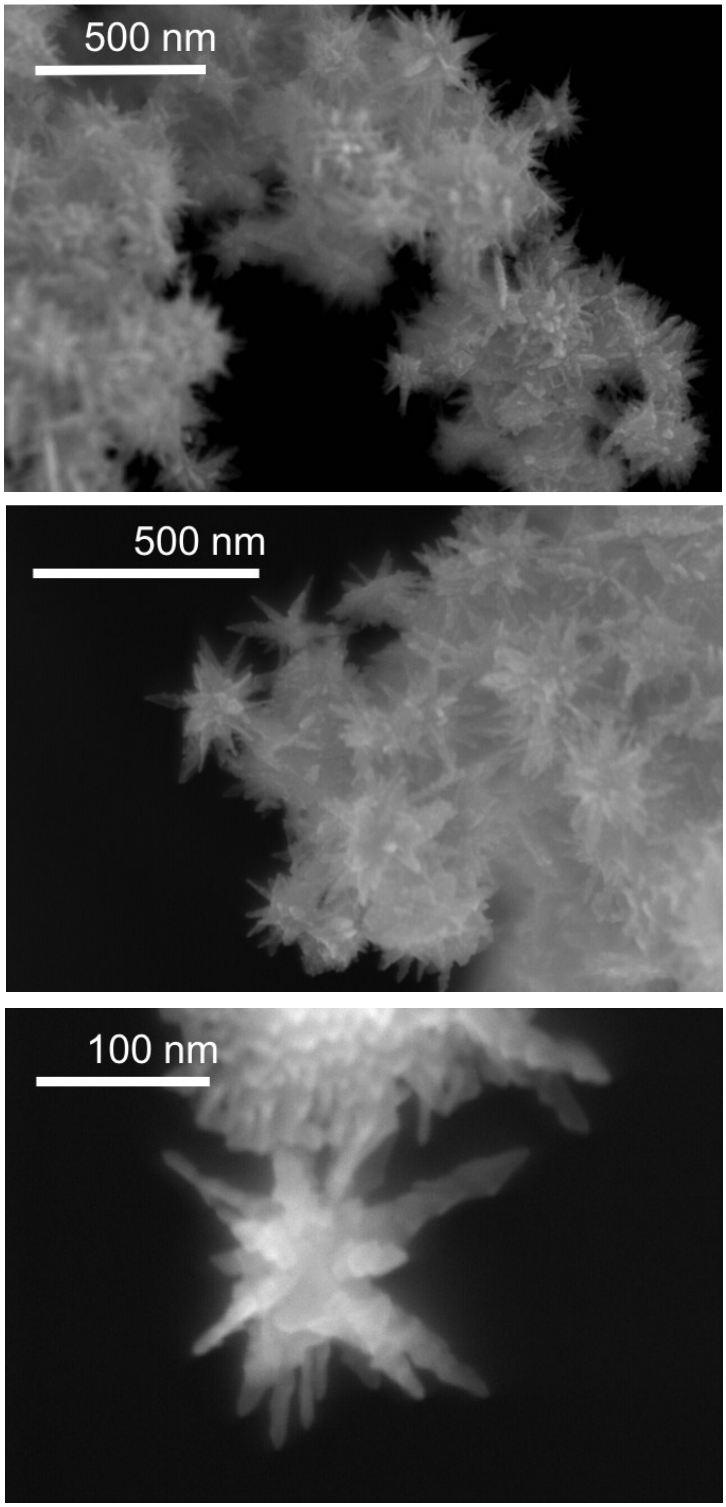

Figure S6. SEM images of Pd BNPs.

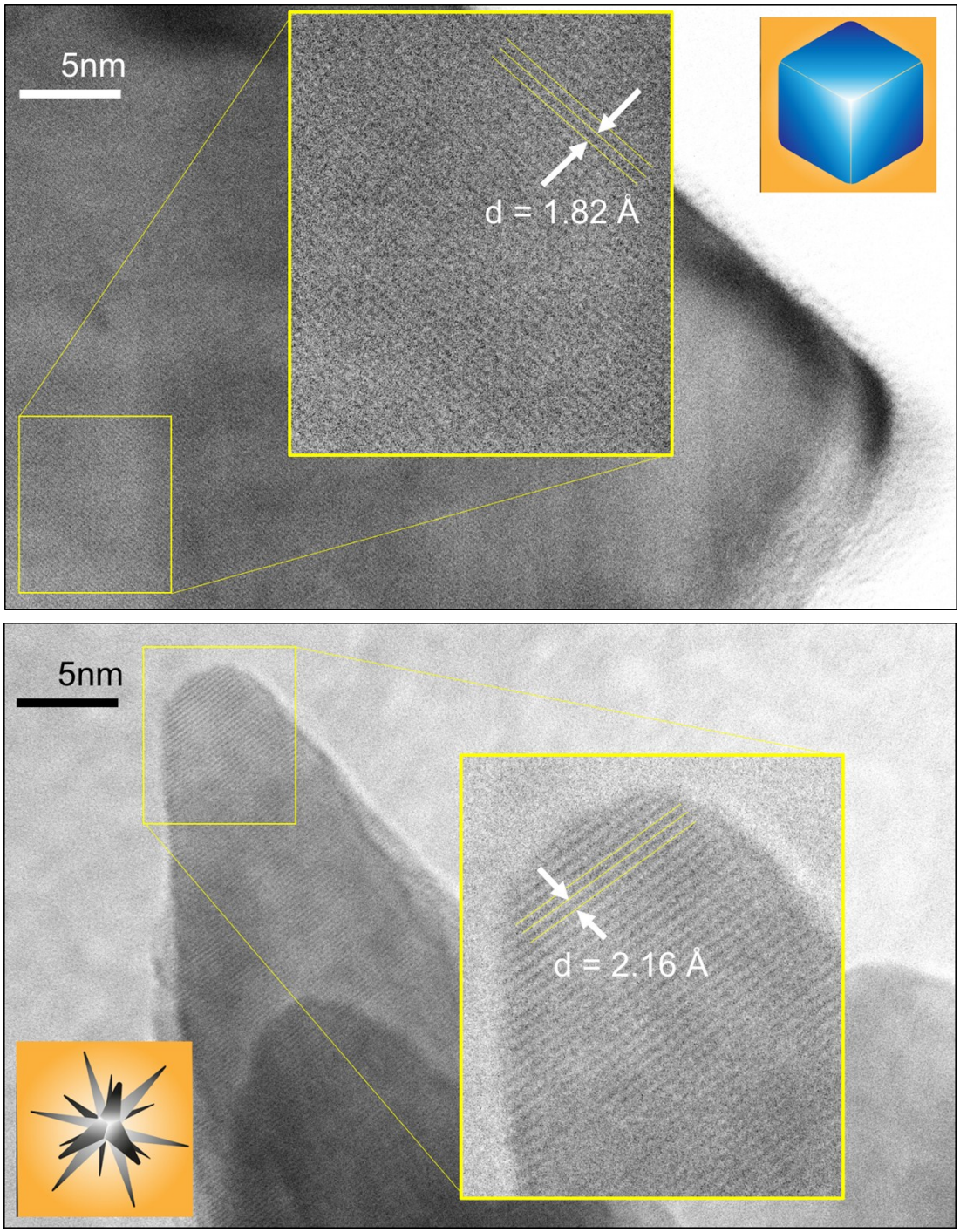

Figure S7. HRTEM images of Pd NCs (top) and Pd BNPs (bottom).

The HRTEM images were used to confirm the presence of high index facets on BNPs. It is evident that NCs surface enclosed by {100} facet appears to be closely packed with calculated value of interatomic distance of 1.82 Å. In the case of BNPs, the interatomic distance is greater and was calculated to be 2.16 Å which may be related to the distance between the exposed edges of higher index facets.

Electrochemical Surface area measurements

For the determination of electrochemically active surface area of electrodes we used stripping charge of saturated CO adlayer. At Pd electrode, CO_{ad} oxidation takes place in the range between -0.65 and -1.2 V vs Ag/AgCl. The net Faradic charge for the oxidation of a saturated CO adlayer (Q_{CO} oxidation) net is determined by the following equation:

$$Q_{net}^{CO\ oxidation} = Q_{total}^{CO\ stripping} - Q_{ox}^{Pd}$$

where $Q_{net}^{CO\ oxidation}$ is the charge density obtained by integration of the CO stripping voltammogram between 0.65 and 1.2 V, Q_{ox}^{Pd} is the charge density obtained by integration of the voltammogram of the CO-free surface between the same potential limits. The ECSA values were estimated assuming that oxidizing a full monolayer of CO on Pd consumes a charge of 420 μC/cm^2. ESCA of electrodes with Pd NPs deposited on carbon paper were determined to be 302.1, 204.6, 187.2, and 154.6 cm^2 for Pd BNPs, NCs, RDs, and Pd black, respectively. Values of current densities were normalized against ECSA in all figures.

Computational Details

The Vienna Ab Initio Simulation Package (VASP)[1] was used for all density functional theory (DFT) calculations. The projector augmented wave (PAW) method[2] was used in conjunctions with the Perdew-Burke-Ernzerhof (PBE)[3] generalized gradient approximation (GGA) exchange correlation functional. (A plane wave basis set was used with Blöchl's all-electron, frozen-core PAW pseudopotentials[4]. A cutoff energy of 500 eV was used. Fermi smearing was used with a width of 0.1 eV. A 5x5x1 Monkhorst-Pack mesh[5] was used for k-point sampling performed on 3x3x3 slabs of Pd(111), Pd(110), Pd(100)**,** and Pd(211). 10 Å of vacuum perpendicular to the surface were included to ensure no mirror image interactions in the z-direction. The Pd_{19} cluster was placed in a periodic box with 10 Å of vacuum in every direction and only the gamma point was sampled. Spin polarization was included as it has previously shown to be important for binding energies on nanoparticles and catalyst surfaces.[6] Structural optimizations were performed with the BFGS algorithm until the structures were fully relaxed (the forces were less than 0.02 eV/atom). Once the slab model's geometry was optimized the bottom two layers were fixed for all subsequent thermodynamic calculations.

Thermodynamic quantities were calculated using the open-source atomic simulation environment (ASE) code[7]. The Gibbs free energies were calculated at standard conditions as shown below:

$$G = H - TS = E_{DFT} + E_{ZPE} + \int_0^{298} C_v dT - TS$$

where E_{DFT} is the electronic energy from DFT calculations, E_{ZPE} is the zero-point vibrational energy, $\int_0^{298} C_v dT$ is the heat capacity, T is the temperature, and ΔS is the entropy. Gas phase molecules were treated using the ideal gas approximation while adsorbates were treated using a harmonic approximation. The DFT calculated energy for CO_2, HCOOH, H_2 and the adsorbed COOH* was corrected by 0.45 eV, 0.20 eV, +0.09eV, and 0.20 eV commonly employed to account for an overestimation by DFT.[8,9] The computational hydrogen electrode model (CHE)[10] was used to calculate the change in Gibbs free energy of reaction, ΔG_{rxn}, between proton coupled electron transfer steps of the CO_2 to HCOOH reaction. To calculate the ΔG_{rxn} at an applied potential, the ΔG_{rxn} was corrected by qU where q is the elementary charge and U is the applied potential with respect to the pH-insensitive RHE.

Additionally, the intermediate Gibbs free energy was calculated as follows, $\Delta G_{intermediates} = G_{CO*/HCOO*} - (E_{Pd} + G_{CO/HCOO})$ where $G_{CO*/HCOO*}$ is the energy of the system with CO or HCOO bound to the Pd surface, E_{Pd} is the energy of the Pd surface (entropic contributions of the solid surface are ignored as they will be far smaller than for the bound intermediates), and G_{co} is the gas phase Gibbs energy of CO and $G_{HCOO} = G_{HCOOH} - ½ G_{H2}$.

Table S1: Gas phase molecules and their thermodynamic quantities (eV).

Molecule	**E_{DFT}**	**ZPE**	**∫CvdT**	**TS**	**G**
H_2O	-14.21	0.56	0.10	0.67	-14.22
CO_2	-22.95	0.31	0.10	0.66	-22.79
H_2	-6.77	0.27	0.09	0.43	-6.76
CO	-14.78	0.13	0.09	0.67	-15.22
HCOOH	-29.87	0.89	0.11	1.05	-29.71

Table S2: Adsorbate molecules and their thermodynamic quantities (eV).

		Pd(100)			
Adsorbates	**E_elec**	**ZPE**	**∫CvdT**	**(-TΔS)**	**G**
Slab	-127.85325				
COOH*	-154.38	0.63	0.10	-0.20	-153.65
CHOO*	-154.51	0.64	0.09	-0.15	-153.94
CO*	-144.16	0.22	0.06	-0.10	-143.97
CO* + OH*	-154.689	0.589	0.103	-0.173	-154.17
		Pd(110)			
Adsorbates	**E_elec**	**ZPE**	**∫CvdT**	**(-TΔS)**	**G**
Slab	-121.30				
COOH*	-148.04	0.65	0.09	-0.18	-147.27
CHOO*	-148.49	0.64	0.09	-0.17	-147.42
CO*	-137.84	0.22	0.06	-0.10	-137.67
CO* + OH*	-148.25	0.59	0.10	-0.18	-147.74
		Pd(111)			
Adsorbates	**E_elec**	**ZPE**	**∫CvdT**	**(-TΔS)**	**G**
Slab	-130.90				
COOH*	-157.41	0.62	0.11	-0.23	-156.71
CHOO*	-157.46	0.64	0.09	-0.15	-156.89
CO*	-147.15	0.22	0.06	-0.10	-146.96
CO* + OH*	-157.81	0.58	0.10	-0.17	-157.30
		Pd(211)			
Adsorbates	**E_elec**	**ZPE**	**∫CvdT**	**(-TΔS)**	**G**
Slab	-130.18				
COOH*	-157.01	0.64	0.09	-0.16	-156.24
CHOO*	-157.08	0.63	0.09	-0.17	-156.53
CO*	-146.57	0.21	0.07	-0.14	-146.44
CO* + OH*	-157.20	0.58	0.11	-0.21	-156.72
		Pd-19			
Adsorbates	**E_elec**	**ZPE**	**∫CvdT**	**(-TΔS)**	**G**
NP	-76.48				
COOH*	-102.90	0.62	0.11	-0.26	-102.23
CHOO*	-103.19	0.61	0.11	-0.24	-102.72
CO*	-92.74	0.22	0.06	-0.10	-92.56
CO* + OH*	-103.37	0.61	0.10	-0.16	-102.83

References

1 Kresse, G.; Furthmüller, J. *Phys. Rev. B* **1996**.

2 Blöchl, P. E. *Phys. Rev. B* **1994**, *50* (24), 17953

3 Ernzerhof, M.; Scuseria, G. E. J. Chem. Phys. 1999, 110 (11), 5029.

4 Kresse, G. Phys. Rev. B 1999, 59 (3), 1758

5 Monkhorst, H. J.; Pack, J. D. Phys. Rev. B 1976, 13 (12), 5188

6 Hansen, H. a.; Varley, J. B.; Peterson, A. a.; Nørskov, J. K. J. Phys. Chem. Lett. 2013, 4 (3), 388

7 Bahn, S. R.; Jacobsen, K. W. Comput. Sci. Eng. 2002, 4 (3), 56

8 Yoo, J. S.; Christensen, R.; Vegge, T.; Nørskov, J. K.; Studt, F. ChemSusChem 2016, 9 (4), 358

9 Christensen, R.; Hansen, H. A.; Vegge, T. *Catal. Sci. Technol.* **2015**, *5* (11), 4946

10 Peterson, A. a.; Abild-Pedersen, F.; Studt, F.; Rossmeisl, J.; Nørskov, J. K. Energy Environ. Sci. 2010, 3 (9), 1311